International Journal of Heat and Mass Transfer 52 (2009) 3169–3175

Contents lists available at ScienceDirect

International Journal of Heat and Mass Transfer

journal homepage: www.elsevier.com/locate/ijhmt

Heat transfer characteristics of a micro-scale impinging slot jet

Kyo Sung Choo [a], Young Jik Youn [a], Sung Jin Kim [a,*], Dae Hee Lee [b]

[a] School of Mechanical, Aerospace & Systems Engineering, Korea Advanced Institute of Science and Technology, Daejeon 305-701, South Korea
[b] School of Mechanical and Automotive Engineering, High Safety Vehicle Core Technology Research Center, Inje University, Gimhae 621-749, South Korea

ARTICLE INFO

Article history:
Received 23 August 2008
Received in revised form 4 February 2009
Accepted 9 February 2009
Available online 28 March 2009

ABSTRACT

In the present study, heat transfer characteristics of a micro-scale slot jet impinging on a heated flat plate are experimentally investigated. The effects of Reynolds numbers (Re = 150–5000) and nozzle-to-plate spacings (Z/d_h = 0.5–10) on the Nusselt number are considered. Based on the experimental results, correlations on the stagnant and average Nusselt numbers for the micro-scale impinging slot jet are developed as a function of Reynolds number and nozzle-to-plate spacing. At Reynolds numbers (Re < 2500), different from the existing results, the present study shows that the heat transfer characteristics of the micro-scale impinging slot jet are similar to those of the macro-scale impinging slot jet. However, at Reynolds numbers ($Re \geqslant 2500$), the present study shows that the heat transfer characteristics of the micro-scale impinging slot jet are different from those of the macro-scale impinging slot jet. Firstly, a maximum local Nusselt number occurs at a shifted peak of about x/d_h = 1.75 under the condition of large nozzle-to-plate spacing ($Z/d_h > 1$), rather than at the stagnation point. Secondly, the effect of the nozzle-to-plate spacing on the Nusselt number is significant. The exponent on Reynolds number is the function of nozzle-to-plate spacing $Nu \propto Re^{f(Z/d_h)}$, rather than a constant value.

1. Introduction

An impinging jet is widely used in many engineering applications for the heating, cooling, and drying of surfaces because it has highly localized heating, cooling, and drying rates. Major industrial applications of the impinging jet include turbine blade cooling, electronic equipment cooling, metal annealing, and textile drying. For this reason, there have been many investigations on the heat transfer characteristics of macro-scale impinging jets in the past decades [1–10]. Martin [1] presented a comprehensive review on impinging jets and provided extensive heat transfer correlations for a single jet and jet arrays.

Recently there has been an interest in applying the impinging jet to small-scale devices as electronic components become smaller and smaller. Shen and Gau [11] conducted an experiment for a micro-scale impinging jet with a slot width of 200 μm. Based on the experimental results, they claimed that the results of the micro-scale impinging slot jet are significantly different from those of the macro-scale slot impinging jet. However, there were two limitations of the study by Shen and Gau [11]. Firstly, the range of the Reynolds number in their study was narrow because the sensor used in the experiment, which was made by using bulk-etching, had a fracture problem under high pressure. The range of the Reynolds number used by Shen and Gau [11] belongs to a laminar flow region. However, the impinging jet is usually used in transition and turbulent flow regions due to high heat transfer rate. Viskanta [2] and Polat et al. [3] indicated that the transition from laminar to turbulent flows occurs at approximately the Reynolds number of Re = 2500. The transition causes a shifted peak and contributes the enhancement of heat transfer in a shear layer. On the other hand, it is impossible to observe the transition phenomena within the range of the Reynolds number used by Shen and Gau [11]. Thus, a study of the heat transfer characteristics of the micro-scale impinging jet at a wide range of Reynolds numbers is needed in order to compare them with those of the macro-scale impinging jet. Secondly, there was a limitation of the measurement accuracy in the study because a heated plate used by Shen and Gau [11] has the silicon substrate with a high lateral conduction. A high lateral conduction of the heated plate distorts the measurement accuracy. Patil and Narayanan [13,14] indicated that the lateral conduction along the heated plate contributed a significant portion to convective heat transfer for the micro-scale circular impinging jet. The lateral conduction in their study has the same order of magnitude as the amount of heat supply to an Inconel foil substrate. The silicon substrate used by Shen and Gau [11] has a higher thermal conductivity than the Inconel foil substrate used by Patil and Narayanan [13,14]. Hence, the effect of the lateral conduction on the measurement accuracy for the former is more crucial than for the latter. Therefore, a heated plate which has a negligible lateral conduction is needed to measure the surface temperature accurately.

* Corresponding author. Tel.: +82 42 350 3043; fax: +82 42 350 8207.
E-mail address: sungjinkim@kaist.ac.kr (S.J. Kim).

0017-9310/$ - see front matter Crown Copyright © 2009 Published by Elsevier Ltd. All rights reserved.
doi:10.1016/j.ijheatmasstransfer.2009.02.015

Nomenclature

A	convective area (m^2)
B	nozzle width (m)
d_h	hydraulic diameter (m)
h	local heat transfer coefficient (W/m^2 K)
I	current passed through the heater (A)
k	thermal conductivity of the heater (W/m K)
k_f	thermal conductivity of air (W/m K)
l	length of the heater (m)
Nu	Nusselt number (hB/k_f)
Nu_0	Nusselt number at stagnation point
q_{cond}	heat conduction from the heater (W)
q_{conv}	heat convection from the heater (W)
q_{gen}	heat generation from the heater (W)
q_{loss}	heat loss from the heater (W)
q_{rad}	heat radiation from the heater (W)
Re	Reynolds number (uB/v)
t	thickness of the heater (m)
T	temperature (°C)
T_{in}	temperature at the jet exit (°C)
T_∞	ambient temperature (°C)
u	jet velocity (m/s)
V	voltage across the heater (V)
w	width of the heater (m)
x	lateral distance from stagnation point (m)
Z	nozzle-to-plate spacing (m)

Greek Symbol

ε	emissivity of the upper heater surface
v	dynamic fluid viscosity (m^2/s)
σ	Stefan Boltzman constant (5.67×10^{-8}, W/m^2K^4)

The purpose of the present study is to find the heat transfer characteristics of the micro-scale impinging jet and to compare them with those of the macro-scale impinging jet at a wide range of Reynolds numbers using a heated plate with a negligible lateral conduction. In the experiment, a very thin gold-coated polyester substrate sheet (called 'gold-film Intrex' according to Lee [10]) was used as the heater. The lateral conduction of the gold-film Intrex is three hundred times lower than that of the silicon substrate used by Shen and Gau [11]. The experimental parameters include a wide range of Reynolds numbers (Re = 150–5000) and nozzle-to-plate spacings (Z/d_h = 0.5–10). Based on the experimental results, correlations for the stagnant and average Nusselt numbers of the micro-scale impinging jet are developed. The correlations as a function of the Reynolds number and the nozzle-to-plate spacing are presented.

2. Experimental apparatus and procedures

A schematic diagram of the experimental apparatus is shown in Fig. 1. The entire apparatus was fixed on an optical table to isolate the vibration. Compressed air passed through a flexible tube and a long straight SUS pipe before entering a micro-scale unconfined slot nozzle. The airflow was supplied by a high-pressure tank to furnish a very clean and steady flow. The flow was then regulated and controlled by a mass flow controller (Brooks 5850E). Its accuracy and repeatability are ±1% and ±0.15%, respectively. The flow velocity at the nozzle exit can be readily found from the mass flow rate and the nozzle exit area. The unconfined slot nozzle has a cross-section area of 0.25 mm × 10 mm with an aspect ratio of 40. The hydraulic diameter of the nozzle is about 0.5 mm. The micro-nozzle was fixed on an X–Y–Z stage made by Thorlabs, Inc. Thus, the nozzle could be moved either parallel or perpendicular to the direction of the jet.

As shown in Fig. 2, the heated flat plate is composed of a balsawood flat plate, a gold-coated film heater with a polymer substrate, E-type thermocouples and two copper electrodes. The 30×30 mm^2 balsawood plate is 0.8 mm thick and has a low thermal conductivity. A Styrofoam insulation plate of $60 \times 60 \times 40$ mm^3 was placed behind the balsawood plate to minimize heat losses. The transparent vacuum-deposited gold-coated film heater, 20 mm long by 10 mm wide, has a polymer substrate thickness of 50 μm and a coated gold thickness of 10 nm. The film heater was glued to the balsawood plate. Two copper-foil strip electrodes with a thickness of 0.1 mm were attached to the film heater. Then, silver paint was applied to establish a good electrical contact between the electrode and the upper surface of the film heater. The electrodes were connected to a DC power supply (HP6555A) in series with a shunt, rated 50 mV and 5 A, allowing adjustable DC voltage to the electrodes. With DC electric current applied to the film heater, a nearly uniform wall heat flux boundary condition was established. In order to obtain the amount of heat generation correctly, the amount of heat generation was obtained under the steady state condition by running the impingement. We started impinging air on the unheated film heater, and applied heat to the film heater. We waited until the variation of the temperature difference between the heater and the nozzle exit air is within 0.2 °C for 10 min. Then we measured the voltage and the resistance across the film in order to obtain electrical energy input accurately. In order to measure the surface temperature, an E-type thermocouple of diameter 80 μm was installed between the balsawood plate and the film heater. A hole with 0.1 mm diameter was made on the balsawood plate to install a thermocouple without a local deflection of the film heater. The temperature distribution on the heated surface was measured using the thermocouple. In order to locate a thermocouple at the center of nozzle exit, we controlled the three axis (X–Y–Z) stage with the spatial resolution of 10 μm. E-type thermocouples were also attached on each face of the Styrofoam to obtain the heat losses. Lastly, the thermocouples were connected to the HP3852A data acquisition system.

3. Data analysis and reduction

The local convective heat transfer coefficient and corresponding Nusselt number for the ith control volume were calculated using the following equation:

$$h_i = \frac{q_{conv,i}}{A_i(T_i - T_{in})}, \quad Nu_i = \frac{h_i B}{k_f} \tag{1}$$

For a given control volume, illustrated in Fig. 3, the convective heat $q_{conv,i}$ from the upper control volume surface was calculated using the following equation:

$$\begin{aligned} q_{conv,i} &= q_{gen,i} + q_{cond,i} - q_{rad,i} \\ &= \left(\frac{fVI - q_{loss}}{A}\right)A_i + (wt)k\left(\frac{dT}{dx}|_{i+1} - \frac{dT}{dx}|_i\right) - \varepsilon_i \sigma A_i (T_i^4 - T_\infty^4) \end{aligned} \tag{2}$$

where the convective area of the ith control volume is $A_i = w(x_{i+1} - x_i)$ and the total heated area is $A = wl$. In Eq. (2), f accounts for non-uniformity factor of the gold-coated film and $f \approx 1$ is usually adopted for small slender shape of the film.

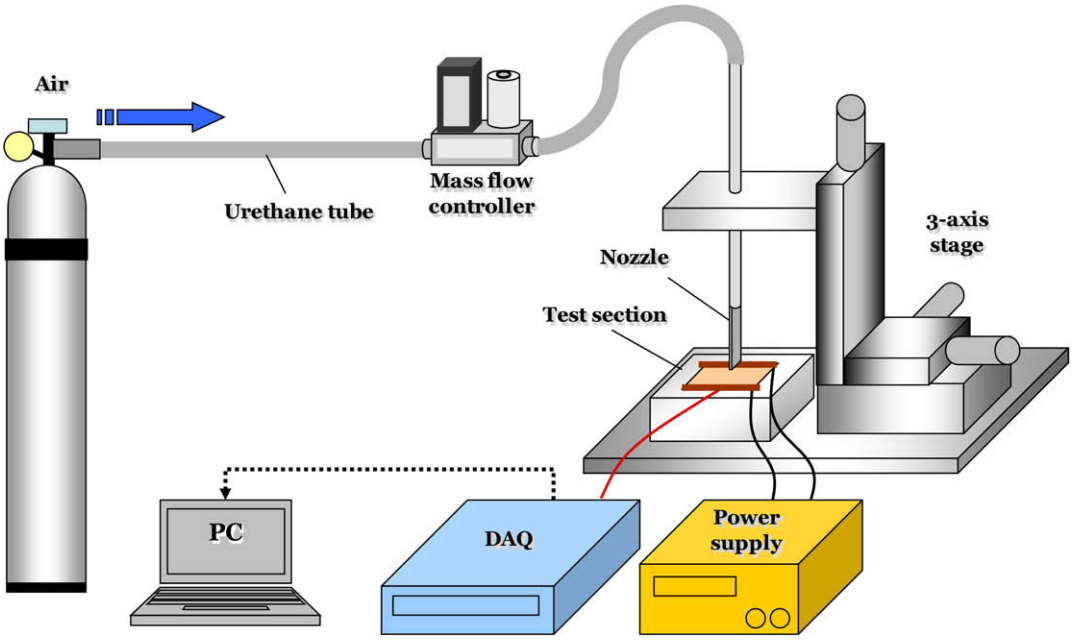

Fig. 1. Schematic diagram of experimental set-up.

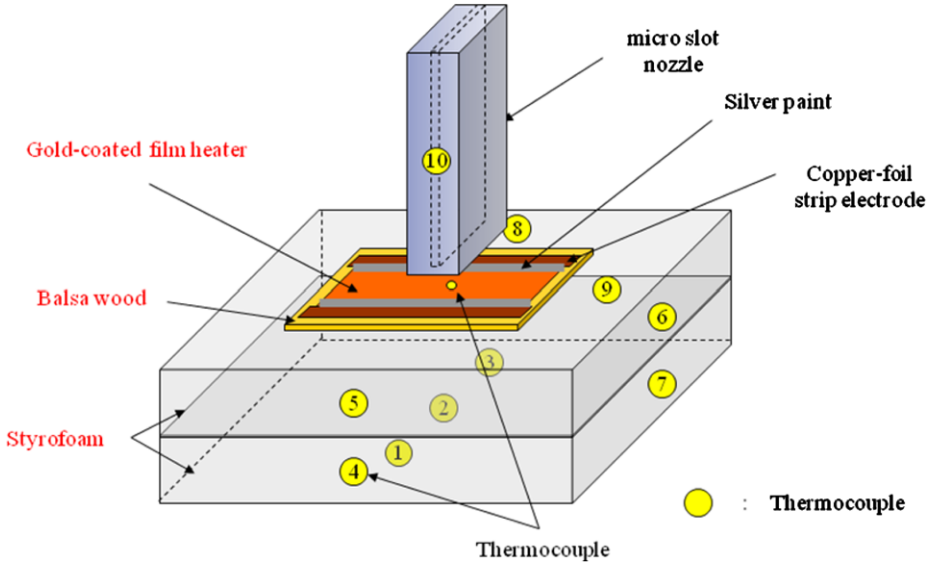

Fig. 2. Test section configuration.

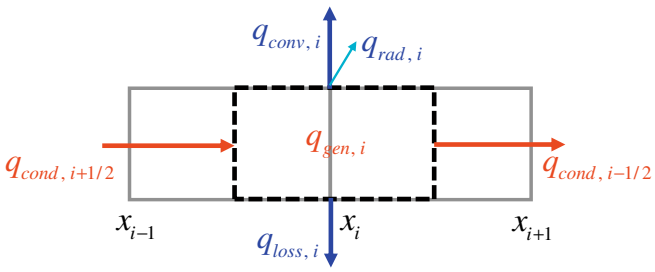

Fig. 3. Segment of control volume of a heater.

In the analysis, the radiation heat $q_{rad,i}$ was calculated from the Stefan-Boltzmann equation and the result is less than 0.5% of the total imposed heat. The heat losses q_{loss} were obtained by measuring the temperature and applying the Nusselt number correlation for free convection on each face of the Styrofoam [15]. The maximum heat losses from the heated surface to the ambient temperature are estimated to be about 5% of the total imposed heat.

The lateral conduction $q_{cond,i}$ was calculated by solving the one-dimensional energy equation along the lateral direction of the plate. A higher lateral conduction distorts the measurement accuracy of the surface temperature. Patil and Narayanan [13,14] indicated that the lateral conduction along a heated plate made a significant contribution to the convective heat for the micro-scale circular impinging jet. The lateral conduction has the same order of magnitude as the amount of heat supply to an Inconel foil substrate with a thermal conductivity of k = 15 W/m K and a thickness of t = 25.4 μm. The silicon substrate used by Shen and Gau [11] had even higher thermal conductivity than the Inconel foil substrate used by Patil and Narayanan [13,14] at k = 150 W/m K, and a thick-

ness of $t = 40$ μm. In present study, a polymer substrate with a thermal conductivity of $k = 0.4$ W/m K and a thickness of $t = 50$ μm was used in order to reduce lateral conduction. The thermal conductivity of the polymer substrate used in this study is twenty times lower than that of the Inconel foil substrate and three hundred times lower than that of the silicon substrate. The lateral conduction in the present study is less than 5% of the total imposed heat.

The uncertainty in the local Nusselt numbers is estimated with a 95 percent confidence level using the methods suggested by Kline and McKlintock [16]. Table 1 showed that the overall uncertainties in the Nusselt number were in the range of 2.62–2.95%.

4. Results and discussion

4.1. Influence of lateral distance

The experimental data of the present study for macro-scale impinging jet were compared with the empirical correlation of Lytle and Webb [17] as a validation process. The circular pipe nozzle has 4 mm inner diameter by 20 cm long was used. For Reynolds numbers in the range $3600 \leqslant Re \leqslant 17{,}300$, the stagnation Nusselt numbers were examined at four nozzle-to-plate spacings of 0.125, 0.25, 0.5 and 1, as shown in Fig. 4. The adopted empirical correlation of Lytle and Webb is $Nu_0 = 0.726\, Re^{0.53}(Z/d_h)^{-0.191}$. As shown in the figure, good agreements between the present data and the previous empirical correlation were observed within ±10%.

In order to find the heat transfer characteristics of the micro-scale impinging jet and compare them with those of the macro-scale impinging jet, the effect of lateral variation of the local Nusselt number was considered. Fig. 5 illustrates the lateral variation of the local Nusselt number at $Z/d_h = 1.5$ for $Re < 2500$. At Reynolds numbers of $Re < 2500$, the local Nusselt number distribution has a bell shape which is similar to that of the macro-scale impinging jet. Fig. 6(a) illustrates the lateral variation of the local Nusselt number at $Z/d_h = 1.5$ for Reynolds numbers of $Re \geqslant 2500$.

At Reynolds numbers of $Re \geqslant 2500$ and $Z/d_h = 1.5$, the local Nusselt number exhibits a shifted peak at around $x/d_h = 1.75$. The local Nusselt number increases with increasing lateral distance from the stagnation point to the shifted peak and decreases monotonically beyond the shifted peak. The lateral variation of the local Nusselt number has a maximum value at the shifted peak location $x/d_h = 1$–2 [6,7,12,17]. As Viskanta [2] put it, there has been considerable speculation and disagreement among investigators as to the physical explanation for the shifted peak. Liu et al. [6] and Lytle and Webb [17] explained that the shifted peak occurred due to the transition from laminar to turbulent. Goldstein et al. [7] explained the shifted peak as the result of a vortex ring. Pence et al. [12] explained that the shifted peak is due to the flow acceleration which is very strong in micro-scale jets because the corresponding exit velocities are very large. The shifted peak in the macro-scale impinging jet was observed under the condition of high Reynolds numbers ($Re \geqslant 40000$) or small nozzle-to-plate spacing ($Z/d_h < 1$) [6,7,17]. In present study, the shifted peak was observed under the condition of low Reynolds numbers ($Re = 2500$–5000) and large nozzle-to-plate spacing ($Z/d_h > 1$). As shown in Fig. 6(a) and (b), the results for the shifted peak in the present study were similar to those of a micro-scale circular impinging jet by Pence et al. [12]. Hence, we strongly believe that the acceleration due to the large velocity is apparently sufficient to induce a shifted peak in the local Nusselt number. To the best of our knowledge, there is no such information on physical explanation of the shifted peak phenomenon in open literature. Further research is required for the occurrence and explanation of the shifted peak. Fig. 6(c) shows that the effect of the secondary peak was diminished as nozzle-to-plate spacing increases. In addition, the end effect (3D) in the nozzle design is an important research topic in micro-scale impinging jet as the reviewer suggested. We expect that the end effect of the micro-scale impinging jet will cause the off-axis peak which is similar to that of the macro-scale impinging jet for a rectangular jet by Zhou and Lee [9]. Further research is required for the end effect (3D) in the nozzle design.

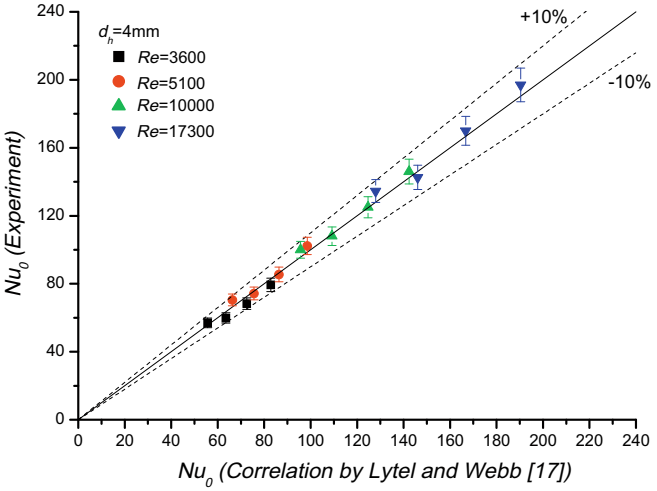

Fig. 4. Correlation and comparison of the stagnation Nusselt number.

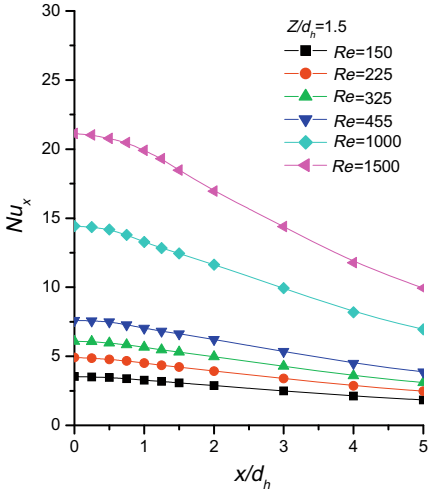

Fig. 5. Lateral variation of the local Nusselt number at $Z/d_h = 1.5$.

Table 1
Uncertainty analysis of the total Nusselt nuber.

Individual measured value		$\left\lvert\frac{\delta_{Xi}}{Nu}\frac{\partial Nu}{\partial_{Xi}}\right\rvert \times 100(\%)$
X_i	Unit	
f	–	1.75–1.9
T_i	°C	1.43–1.45
T_{in}	°C	0.93–1.05
V	V	0.36–0.64
I	A	0.23–0.41
q_{loss}	W	0.81–0.97
B	m	0.02–0.03
A	m^2	0.07
k	W/m K	0.06
e	–	0.19–0.6

Total uncertainty: $\delta Nu/Nu = 2.62$–2.95%.

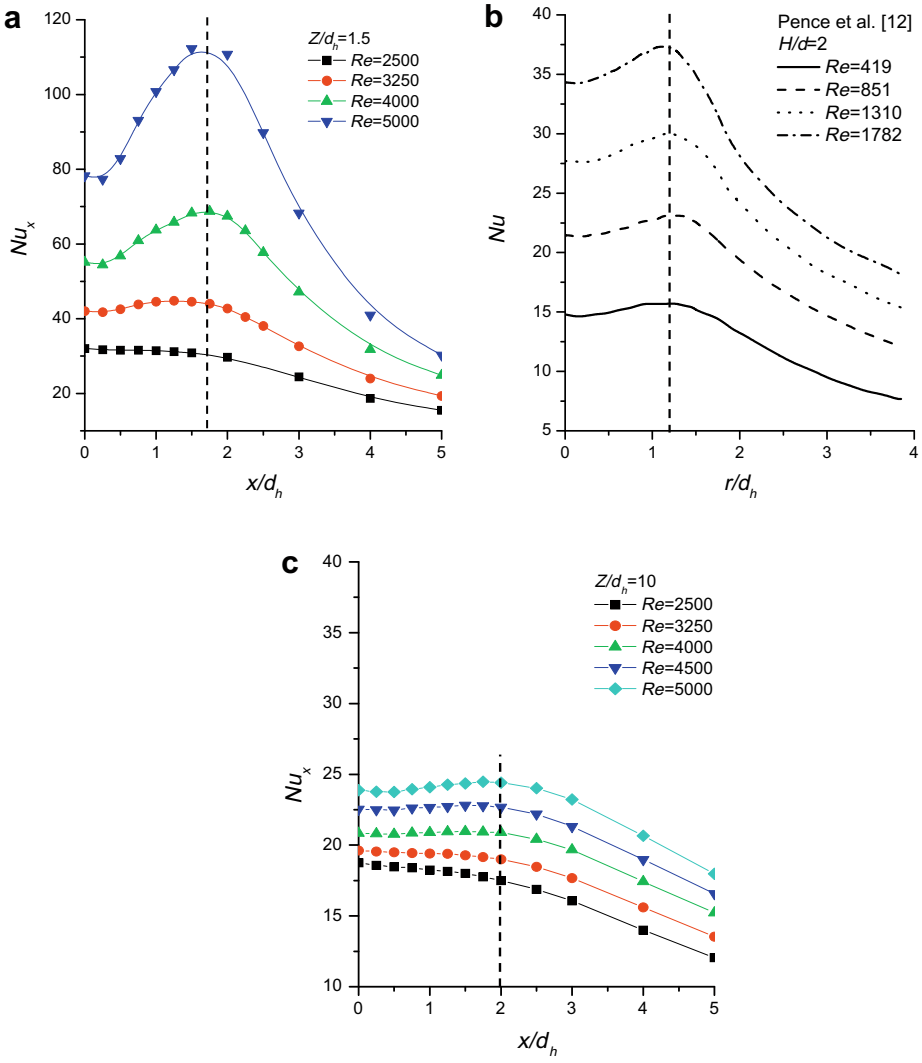

Fig. 6. Lateral variation of the local Nusselt number: (a) present data at $Z/d_h = 1.5$ (b) Pence et al. [12] (c) present data at $Z/d_h = 10$.

4.2. Influence of nozzle-to-plate spacing

The variation of the stagnant Nusselt number for nozzle-to-plate spacing is shown in Fig. 7. It can be seen from this figure that the variation of the stagnant Nusselt number (Nu_0) with respect to the nozzle-to-plate spacing (Z/d_h) exhibits a complex nature that may not be monotonic depending on the Reynolds number. At Reynolds numbers of $Re < 3250$, there is a hump at $Z/d_h = 3$–6, as can be seen in Fig. 7(a). The stagnant Nusselt number initially decreases with increasing axial distance from the stagnation point to the hump. It decreases beyond the hump. The hump moves from $Z/d_h = 6$ to 2 as the Reynolds number increases. A similar non-monotonic behavior was also observed for the macro-scale slot impinging jets investigated by Gardon and Akfirat [4,5] and Sparrow and Wong [8] at Reynolds numbers of $Re < 3250$.

At Reynolds numbers of $Re \geqslant 3250$, a maximum stagnant Nusselt number occurs at $Z/d_h = 2$, as can be seen in Fig. 7(b). The stagnant Nusselt number increases as the nozzle-to-plate spacing increases from the stagnation point to the location of the maximum stagnant Nusselt number. It decreases beyond the location of the maximum stagnant Nusselt number. This trend is consistent with the results of Martin [1], Gardon and Akfirat [4,5], and Zhou and Lee [9] at Reynolds numbers of $Re \geqslant 3250$. It is well known that the variation of the stagnant Nusselt number according to nozzle-to-plate spacing is mainly affected by the potential core [4,5].

4.3. Correlations for a micro-scale impinging jet

In order to develop correlations for the micro-scale impinging jet, the stagnant Nusselt numbers for the nozzle-to-plate spacings of 2, 3, 5, and 10 are presented in Fig. 8. The correlations are divided into a lower Reynolds number region ($Re < 2500$) and a higher Reynolds number region ($Re \geqslant 2500$) since the heat transfer characteristics of the impinging jet are different between them, as mentioned in Sections 4.1 and 4.2 and Refs. [2–5]. The correlations of the stagnant Nusselt number for the micro-scale impinging jet have the following form:at lower Reynolds numbers ($150 \leqslant Re < 2500$),

$$Nu_0 = 0.1Re^{0.74}\left(\frac{Z}{d_h}\right)^{-0.15} \tag{3}$$

at higher Reynolds numbers ($2500 \leqslant Re \leqslant 5000$),

$$Nu_0 = 2.11 \times 10^{-4} Re^{m_1}\left(\frac{Z}{d_h}\right)^{3.6} \tag{4}$$

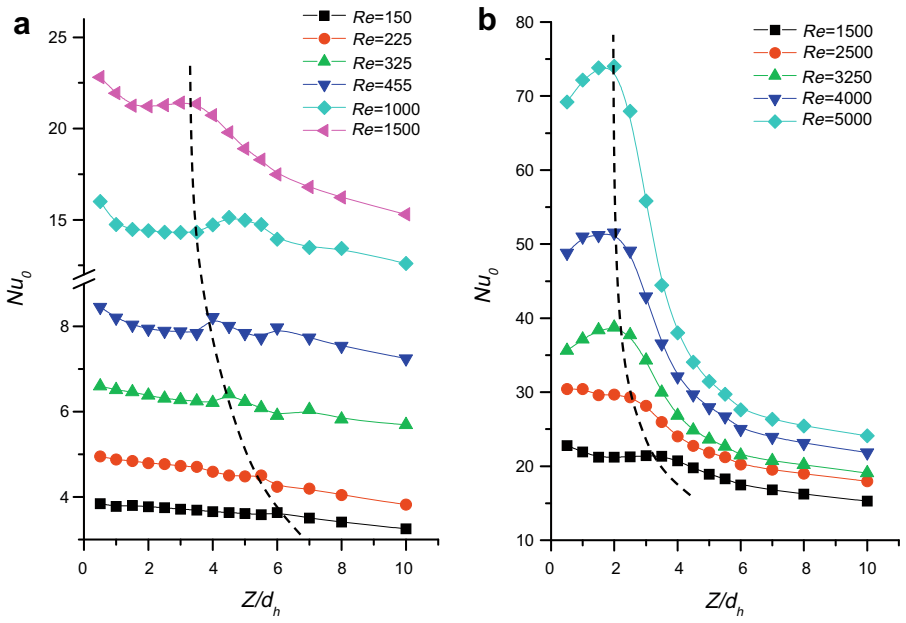

Fig. 7. Variation of the stagnation Nusselt number with nozzle-to-plate spacing: (a) $150 \leqslant Re \leqslant 1500$ and (b) $1500 \leqslant Re \leqslant 5000$.

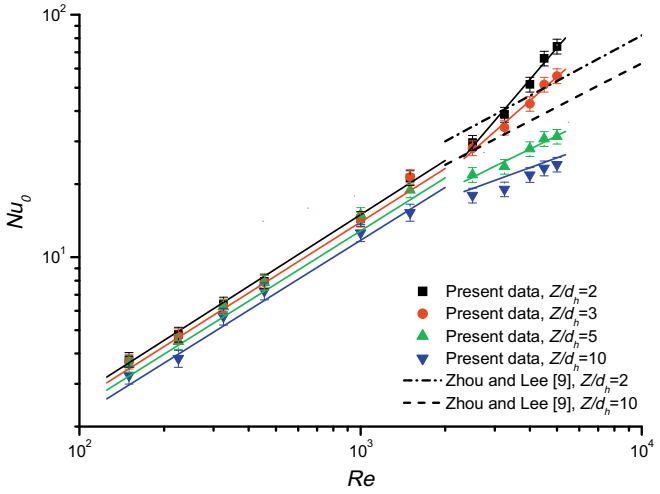

Fig. 8. Correlation of the stagnation Nusselt number at $Z/d_h = 2, 3, 5, 10$.

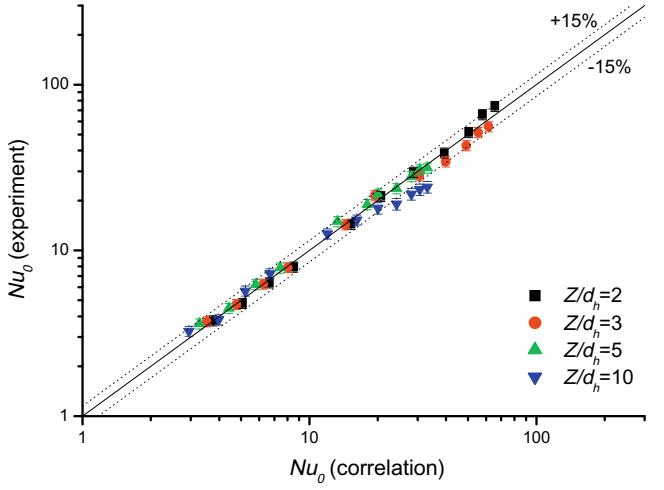

Fig. 9. Comparison between the stagnant Nusselt number obtained from the correlations of Eqs. (3) and (4) and that from experimental results.

with

$$m_1 = 1.618 - 0.236(Z/d_h) + 0.01144(Z/d_h)^2 \quad (5)$$

Both of the above correlations can be used for $0 \leqslant Z/d_h \leqslant 5$. The correlations of the stagnant Nusselt number were compared with the experimental results, and match with the experimental results to within ±15%, as shown in Fig. 9. At lower Reynolds numbers of $Re < 2500$, the exponent on the Reynolds number has a constant value of 0.74 in Eq. (3), and also the exponent on the nozzle-to-plate spacing has a constant value of −0.15. The constant values of the exponents on the Reynolds number and the nozzle-to-plate spacing of the present data are similar to those of the macro-scale impinging jet as shown in Fig. 8. However, at higher Reynolds numbers of $Re \geqslant 2500$, the exponent on the Reynolds number of a micro-scale impinging jet is a function of the nozzle-to-plate spacing, while that of a macro-scale impinging jet is a constant value [4–9]. Namely, as shown in Fig. 8, the effect of the nozzle-to-plate spacing on heat transfer characteristics for the micro-scale impinging jet is more significant than that of the macro-scale impinging jet. As mentioned in Section 4.1, the reason for this is the strong flow acceleration due to the very large exit velocities.

Correlations of the average Nusselt number for the micro-scale slot impinging jet have the following form:
at lower Reynolds numbers ($150 \leqslant Re < 2500$),

$$Nu_{avg} = 0.0784 Re^{0.74} \left(\frac{Z}{d_h}\right)^{-0.15} \quad (6)$$

at higher Reynolds numbers ($2500 \leqslant Re \leqslant 5000$),

$$Nu_{avg} = 1.07 \times 10^{-5} Re^{m_2} \left(\frac{Z}{d_h}\right)^{4.5} \quad (7)$$

with

$$m_2 = 2.015 - 0.294(Z/d_h) + 0.0142(Z/d_h)^2 \quad (8)$$

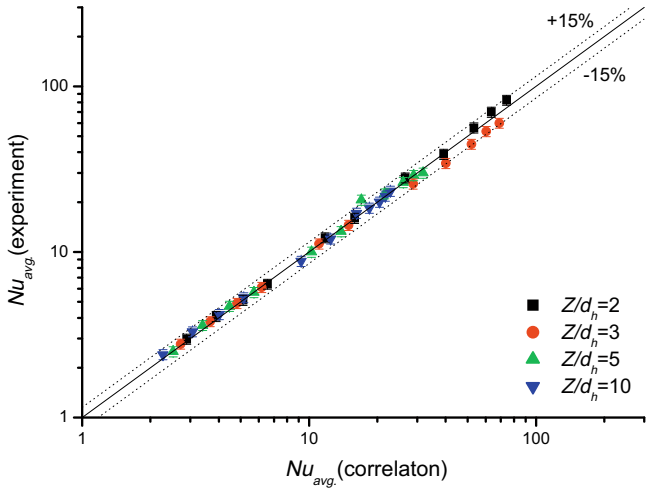

Fig. 10. Comparison between the average Nusselt number obtained from the correlations of Eqs. (6) and (7) and that from experimental results.

Both of the above correlations can be used for $0 \leqslant x/d_h \leqslant 5$ and $0 \leqslant Z/d_h \leqslant 10$. The correlations of the average Nusselt number match with the experimental results to within ±15%, as shown in Fig. 10.

5. Conclusion

In this paper, heat transfer characteristics of a micro-scale slot impinging jet were experimentally investigated. In order to measure the surface temperature accurately, a polymer substrate heater with low lateral conduction was used since a higher lateral conduction in the heated plate distorts the measurement accuracy. The experimental parameters included a jet width of $B = 250$ μm, and a wide range of Reynolds numbers ($Re = 150$–5000) and dimensionless nozzle-to-plate spacings ($Z/d_h = 0.5$–10). Based on the experimental results, correlations for the stagnant and average Nusselt numbers of the micro-scale impinging jet were suggested. The correlations were presented as a function of the Reynolds number and the nozzle-to-plate spacing, $Nu \propto CRe^m(Z/d_h)^n$. At Reynolds numbers ($Re < 2500$), different from the existing results, the present study shows that the heat transfer characteristics of the micro-scale impinging slot jet are similar to those of the macro-scale impinging slot jet. However, at Reynolds numbers ($Re \geqslant 2500$), the micro-scale impinging jet and the macro-scale impinging jet have different heat transfer characteristics. Firstly, a maximum local Nusselt number occurs at a shifted peak of about $x/d_h = 1.75$ under the condition of larger nozzle-to-plate spacing ($Z/d_h > 1$), rather than at the stagnation point of $x/d_h = 0$. Secondly, the effect of the nozzle-to-plate spacing on heat transfer characteristics is significant. The exponent on the Reynolds number is the function of the nozzle-to-plate spacing $Nu \propto Re^{f(Z/d_h)}$, rather than a constant value.

Acknowledgement

This work was supported by the Korea Science and Engineering Foundation (KOSEF) through the National Research Lab. Program funded by the Ministry of Science and Technology (No. M10600000224O6J000022410).

References

[1] H. Martin, Heat and mass transfer between impinging gas jets and solid surface, Adv. Heat Transfer 13 (1977) 1–60.
[2] R. Viskanta, Heat transfer to impinging isothermal gas and flame jets, Exp. Therm. Fluid Sci. 6 (1) (1993) 111–134.
[3] S. Polat, B. Huang, A.S. Majumdar, W.J.M. Douglas, Numerical flow and heat transfer under impinging jets: A Review, Ann. Rev. Num. Fluid Mech. Heat Transfer 2 (1989) 157–197.
[4] R. Gardon, J.C. Akfirat, Heat transfer characteristics of impinging two dimensional air jets, J. Heat Transfer 88 (1966) 101–108.
[5] R. Gardon, J.C. Akfirat, The role of turbulence in determining the heat transfer characteristics of impinging jets, Int. J. Heat Mass Transfer 8 (1965) 1261–1272.
[6] Q. Liu, A.K. Sleiti, J.S. Kapat, Application of pressure and temperature sensitive paints for study of heat transfer to a circular impinging air jet, Int. J. Thermal Sci. 47 (2008) 749–757.
[7] R.J. Goldstein, A.I. Behbahani, K. Kieger Heppelmann, Streamwise distribution of the recovery factor and the local heat transfer coefficient to an impinging circular air jet, Int. J. Heat Mass Transfer 29 (1986) 1227–1235.
[8] E.M. Sparrow, T.C. Wong, Impingement transfer coefficients due to initially laminar slot jets, Int. J. Heat Mass Transfer 18 (4) (1975) 597–605.
[9] D.W. Zhou, S.J. Lee, Forced convective heat transfer with impinging rectangular jets, Int. J. Heat Mass Transfer 50 (2007) 1916–1926.
[10] D.H. Lee, Y.S. Chung, D.S. Kim, Turbulent flow and heat transfer measurements on a curved surface with a fully developed round impinging jet, Int. J. Heat Fluid Flow 40 (1997) 160–169.
[11] C.H. Shen, C. Gau, Heat exchanger fabrication with arrays of sensors and heaters with its micro-scale impingement cooling process analysis and measurements, Sensor. Actuat. A 114 (2004) 154–162.
[12] D.V. Pence, P.A. Boeschoten, J.A. Liburdy, Simulation of compressible micro-scale jet impingement heat transfer, J. Heat Transfer 125 (2003) 447–453.
[13] V.A. Patil, V. Narayanan, Spatially resolved heat transfer rates in an impinging circular microscale jet, Microscale Thermophys. Eng. 9 (2005) 183–197.
[14] V.A. Patil, V. Narayanan, Application of heated-thin foil thermography technique to external convective microscale flows, Meas. Sci. Technol. 16 (2005) 472–476.
[15] F.P. Incropera, D.P. DeWitt, Introduction to Heat Transfer, 4th ed., John Wiley & Sons, Inc, New York, NY, 2002.
[16] S.J. Kline, F.A. McClintock, Describing uncertainties in single sample experiments, Mech. Eng. 75 (1) (1953) 3–8.
[17] D. Lytle, B.W. Webb, Air jet impingement heat transfer at low nozzle-plate spacings, Int. J. Heat Mass Transfer 37 (1994) 1687–1697.